Coupled CFD-DEM Model for a Pneumatic Conveying System

Jacob R. Madden[1]

***Abstract*—Pneumatic conveying systems are used to facilitate bulk movement of granular or powder materials in many industries (mining, chemical, agricultural, etc), and several numerical modeling techniques exist to characterize their behavior. This paper presents the preliminary work completed on a coupled CFD-DEM model, used to predict bulk particle movement due to gas expansion into a hard vacuum, assuming cohesive, homogeneous particles and isentropic, incompressible, turbulent gas flow. This model was developed using open source modeling software (OpenFOAM, LIGGHTS, CFDEMcoupling), and detailed explanations are provided for model parameters and assumptions for the fluid, particle, and coupling states. Preliminary results indicate that this low-fidelity model successfully validates previously completed hardware testing, with potential to significantly accelerate pneumatic system design workflow by reducing the physical testing required to iterate on designs.**

***Index Terms*—Pneumatic Conveying, Numerical Model, OpenFOAM, CFD-DEM, LIGGGHTS, Pneumatic System Design**

I. Introduction

Numerical models are commonly used to study the physical and thermal interactions between particles and fluids in multiphase systems. These fluid-particle interactions can be simulated using various modeling techniques, depending on the specific system properties and desired model outputs. In any case, the model depends on characterizing the conservation of mass, momentum, and energy in the system with varying degrees of fidelity depending on the physical assumptions and numerical model.

One method commonly used in the analysis of pneumatic conveying systems is the coupled Computational Fluid Dynamics - Discrete Element Method (CFD-DEM) approach, an Eularian-Lagragian modeling method which analyzes a continuum fluid state using standard computational fluid dynamics techniques and tracks individual particles using the discrete element method [1]. In this technique, the Navier-Stokes partial differential equations are resolved over a mesh grid to generate locally averaged fluid state vectors for each cell using a CFD solver. Simultaneously, explicit dynamic ordinary differential equations are resolved for each individual particle to generate particle state vectors using a DEM solver. The fluid-particle states are ”coupled” via transfer of data between CFD and DEM solvers at defined intervals [1].

This report describes a coupled CFD-DEM model for a pneumatic transfer system, as seen in Fig. (1). The physical system represents a particle transfer mechanism, in which a loosely packed bed of cohesive particles with zero initial velocity are transported through the piping network due to pressure differential and drag force of a gaseous fluid flow which originates from a pneumatic supply. The initial system state can be modeled using a packed bed model in the annulus, the dynamics of which are dominated by a pressure differential. Once this differential exceeds a certain threshold, bed movement begins and fluid drag force begins moving the particles into a vertical conveying system. As the particles are conveyed into the downstream pipe network, particle momentum dominates the system dynamics [2].

This paper documents the preliminary numerical model developed to characterize this pneumatic conveying behavior and qualitatively validate previous hardware testing. This paper will review the fundamentals of modeling two-phase fluid-particle systems, summarize the governing equations of the system analyzed here, describe the numerical model and techniques used for analysis, and present the results of preliminary simulations. The work completed here forms the foundation for more detailed future modeling of hard-vacuum environment pneumatic conveying systems.

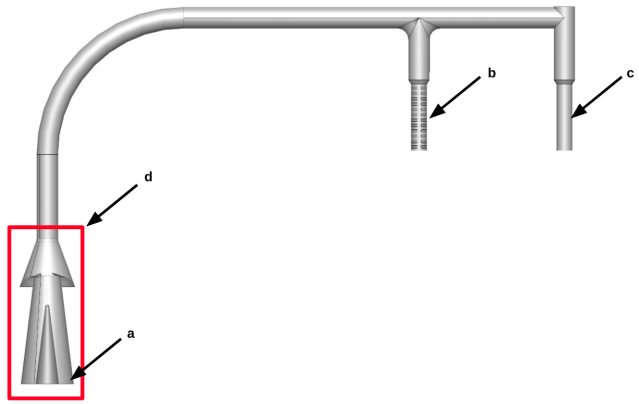

Fig. 1. Physical system used for simulation of numerical model: (a) Inlet annulus (b) Outlet venting to vacuum (c) Secondary chamber (no vents) (d) Reduced system geometry section

II. Prior Work

Numerical modeling of two-phase systems can be generally categorized by the length scales of the fluid and particle states considered. The formulation of conservation equations and closure laws depend on whether the states are taken as discrete or continuum, and the resultant averaging assumptions. Three of the primary modeling approaches are the two-fluid model (TFM), direct simulation-discrete element method (DNS-DEM), and computational fluid dynamics-discrete element model (CFD-DEM) [1].

[1]J.R. Madden is with the Department of Aerospace & Mechanical Engineering, University of Southern California, USA. jrmadden@usc.edu

The two-fluid model assumes both fluid and particle are in the meso-scale and of continuum phase (Eularian-Eularian), using locally averaged Navier-Stokes and continuity equations to compute properties across each cell, and applying semi-empirical closure laws to capture particle motion [3]. This model is valued for its reduced computational workload when modeling a large number of particles, but often fails to accurately capture bulk particle motion because of the use of empirical relations [4].

The direct numerical simulation-discrete element (DNS-DEM) model uses smaller grid size for fluids, and surface stresses on each particle due to fluid flow are directly computed using Navier-Stokes, meaning that empirical correlations are not required to capture drag and lift [1]. However, the extremely fine mesh and small time scale means that this approach is computationally expensive and non realistic for large-scale simulations with many particles or large computational domains [5].

The CFD-DEM model blends aspects of the previous two approaches, using a continuum fluid mesh with discrete particle dynamics (Eularian-Lagrangian). Here, locally averaged Navier-Stokes and continuity equations are used to compute fluid properties across each cell, and particle dynamics are directly resolved, with momentum exchange occurring between phases due to the volume fraction of particles within each fluid cell [1]. This model balances the need for more accurate resolution of particle dynamics and bulk movement with the computational workload required for the DNS approach. For this reason, the CFD-DEM modeling approach was chosen for use in this simulation.

The system analyzed here operates under vacuum condition, as gas is evacuated out of the pipe network into a vacuum chamber. Although literature exists on the empirical formulation of one-dimensional pressure drop relations for vacuum pneumatic conveying [6], [7], small-scale vacuum die-filling [8], [9], [10], particle flowability in vacuum [11], and spouting of particles under vacuum [12], this author has found scarce literature on CFD-DEM modeling of hard-vacuum conveying systems through a pipe network. This paper will focus on this topic, specifically for use in predicting bulk movement of particles through the network.

III. Simulation Model

A. Governing Equations

There two primary models accepted for use in CFD-DEM modeling are referred to as Model A or Model B. The full theoretical treatment and derivation of these models can be found in [13]. The relevant findings will be summarized here.

The general governing equations for the particle phase can be seen in Eqn 1 and Eqn 2. These describe the translational and rotational motion of each particle in the system, where particle-fluid interaction force is given by f_{pf}, inter-particle elastic and damping forces are given by f_c and f_d, respectively, and inter-particle tangential moments and and rolling friction are given by M_t and M_r, respectively [13]. Note that the particle-fluid interaction force, f_p, has a different formulation depending on the model used.

$$m_i \frac{d\mathbf{v}_i}{dt} = \mathbf{f}_{pf,i} + \sum_{j=1}^{k_c} \left(\mathbf{f}_{c,ij} + \mathbf{f}_{d,ij}\right) + m_i \mathbf{g} \tag{1}$$

$$I_i \frac{d\omega_i}{dt} = \sum_{j=1}^{k_c} \left(\mathbf{M}_{t,ij} + \mathbf{M}_{r,ij}\right) \tag{2}$$

The Navier-Stokes equations govern flow in the fluid phase, and under the continuum phase assumption here, governing equations are derived using a local averaging method over each cell, resulting in mass conservation (Eqn. 3) and momentum conservation (Eqn. 4) equations. Note that the equations shown here are for Model A [13].

$$\delta(\varepsilon_f)/\delta t + \nabla \cdot (\varepsilon_f \mathbf{u}) = 0 \tag{3}$$

$$\delta(\rho_f \varepsilon_f \mathbf{u})/\delta t + \nabla \cdot (\rho_f \varepsilon_f \mathbf{u}\ \mathbf{u}) = -\varepsilon_f \nabla p - \mathbf{F}_{pf} + \varepsilon_f \nabla \boldsymbol{\tau} + \rho_f \varepsilon_f \mathbf{g} \tag{4}$$

The particle-fluid interaction forces, f_{pf} in Eqn. (1) and F_{pf} in Eqn. (4), differ depending on the model implemented. In model B, a non-dimensional term which represents the magnitude of the fluid acceleration is introduced, in order to account for several undetermined terms in the momentum conservation equations. As this term approaches zero, a simplified solid phase equation can be derived. However, this rests on the assumption that fluid flow is steady and uniform, which is not the case in general CFD-DEM problems, or in the system analyzed here. In model A, no assumptions are made regarding the fluid flow properties, so it is the more generally accepted model use case, and is the one implemented here. Then, the formulation for the particle-fluid interaction forces as described in Model A are given by Eqn. (5) and (6), where $\mathbf{f}_d$ is drag force, $\mathbf{f}_{\nabla p}$ is pressure gradient force, $\mathbf{f}_{\nabla \tau}$ is viscous force force, and f'' is the sum of non-dominant particle-fluid interaction forces, such as Basset force, Saffman force, Magnus force, etc [13].

$$\mathbf{F}_{pf} = \frac{1}{\Delta V)} \left(\mathbf{f}_d + \mathbf{f''}\right) \tag{5}$$

$$\mathbf{f}_{pf} = \mathbf{f}_d + \mathbf{f}_{\nabla p} + \mathbf{f}_{pf} + \boldsymbol{\nabla \tau}_{pf} + \mathbf{f''} \tag{6}$$

B. Modeling Software

Several open-source software packages and C++ toolboxes were used to implement the underlying model. For simulation of the CFD and fluids calculations, the well-known OpenFOAM (Open-source Field Operation and Manipulation) libraries were used. This toolbox includes various applications and libraries, but the primary structure is organized as seen in Fig. (2) [14]. A system folder includes the main simulation control files which dictate the case time interval, step, and output file properties (*controlDict*), finite volume discretization method and parameters (*fvSchemes*), and equations solvers and algorithms for each fluid property (*fvSolution*). A constant folder holds dictionaries with parameters for turbulence, thermophysical, or transport models, as well as meshing data. The mesh used for the computational domain can be generated using OpenFOAM meshing utilities and applications, such as *snappyHexMesh* (used here), or pre-generated in an external

pre-processing software and converted into an OpenFOAM-readable mesh. Finally, time folders hold initial conditions and boundary field conditions for the domain (ie. 0 case folder) and data for each time interval.

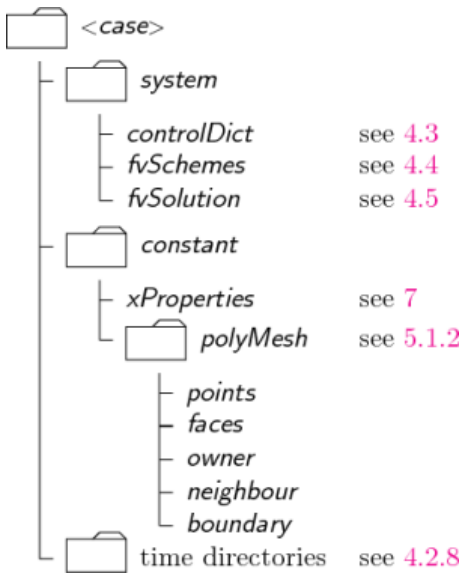

Fig. 2. OpenFOAM case directory structure: *System* sub-directory, which includes discretization techniques, CFD approach, and matrix solvers; *Constant* sub-directory includes meshing data and fluid properties; *Time* sub-directories holding data from each solution timestep

For the DEM modeling, the open-source software LIGGGHTS was used (LAMMPS improved for general granular and granular heat transfer simulations), where LAMMPS is a classical molecular dynamics simulator, developed at Sandia National Labs for materials modeling [15]. This model executes by reading commands from a base input script, as defined by the user, which includes the particle time step, particle property definitions, insertion domain and boundaries using user-defined mesh geometry, cohesion model parameters, external force field definitions (ie. gravity), output settings (defining properties to be saved), and the time-step integration step which repeats until the simulation finishes.

The coupling between the OpenFOAM CFD and LIGGGHTS DEM models was accomplished using the open-source CFDEMcoupling framework, which transfers data between simulation models at set intervals to allow for unresolved coupling. For the fluid phase, this is accomplished by introducing a volume fraction term into the Navier Stokes equations, to account for the presence of particles within each fluid differential volume, as described in the *Governing Equations* section. For the particles, a drag-law force model is introduced to account for the fluid flow.

Meshing for both CFD and DEM sub-models was completed using the open-source Salome software. The base pneumatic conveying system geometry was greatly simplified, by removing complex geometric features inside the piping network, heavily filleting sharp edges, combining transitional pipe sections into smooth faces, and completely removing all external features from the base CAD design. This allowed for an optimized CFD tetrahedral mesh, suitable for this preliminary hardware validation testing. Significant work was undertaken to optimize the feature geometry for a structured hexagonal mesh and a preliminary hex-tet mesh of the initial chamber components was completed successfully, Fig. (3).

C. CFD Sub-Model

The fluids model in this simulation uses a PISO (Pressure Implicit with Splitting of Operators) algorithm to solve the Navier Stokes equations, using three PISO corrector loops to improve convergence. In the PISO algorithm, the fluid pressure and velocity are the dependent variables, and the "splitting" refers to breaking the solutions process into steps which decouple the operations in the discretized momentum and pressure equations (ensuring that these decoupled equations closely approximate the exact solution) [16]. Note that in this method, the pressure equation is obtained from the discretized form of the continuity and momentum equations, rather than discretizing a pressure equation derived from the differential form of these equations. This ensures that the calculated pressure field is consistent with the momentum and continuity equations.

Using the finite-difference method and an Euler implicit time discretization scheme, the momentum and continuity equations for incompressible flow can be discretized to Eqn. (7) and (8), which define the velocity and pressure fields after manipulation. There are several important notes here: First, this method holds for fully compressible fluid flow and with other coupled transport equations (such as the $k-\varepsilon$ turbulence model), and this method is valid for any discretization scheme used. Here, H is the finite-difference operator for spatial convective and diffusive momentum flux, and Δ is the finite-difference equivalent of (d/dx_i) [16].

$$\frac{\rho}{\delta t}\left(u^{n+1}-un\right)=H(u^{n+1})-\Delta p^{n+1}+S \tag{7}$$

$$\Delta u^{n+1}=0 \tag{8}$$

The general algorithm for a PISO method, using the equations above, is outlined as follows. First, the discretized momentum equation is solved implicitly to compute an intermediate velocity field using the current pressure field (the "momentum predictor" step). Then, a pressure correction equation is solved using this velocity field, and then used to correct the velocities ("corrector" step one). Then, the updated pressure and velocity fields are used along with the intermediary fields in a second correction loop to solve for the final pressure and velocities ("corrector" step two). This PISO algorithm can be repeated until the residuals meet the specified requirements [17]. Under-relaxation of the velocity and pressure correction factors promote convergence, so a balance must be struck between computational time and accuracy.

The preconditioned conjugate gradient method (and preconditioned biconjugate gradient method) are used to iteratively solve the matrix equations in the PISO algorithm outlined above. For a general system, Ax = b, these methods use the gradient of a quadratic function associated with the linear system to solve for x such that the residual (r = b - Ax) is reduced to a value within a specified tolerance [18]. After the

CFD solver converges during each time step, the cell averaged pressure and velocity data is passed to the DEM solver.

The numerical schemes for the terms in the model equations (continuity, momentum, and closure) are defined as follows. The first time derivative is discretized using the Crank-Nicolson method, a second-order, implicit finite-difference method which is unconditionally stable. A standard finite volume discretization scheme is selected to compute gradient terms, using linear interpolation of values from cell centers to the faces (used to calculate surface fluxes). For all divergence terms (besides the Laplacian operator), the standard finite volume discretization scheme is again used, with the exception of $k-\varepsilon$ turbulence values, which are computed using a bounded upwind method to improve stability at the expense of accuracy. The Laplacian operator also uses a standard finite volume discretization, with an additional correction term to account for the non-orthogonality of the surface normal gradient of tetrahedron cells.

The time step for the CFD simulation can be estimated by using Courant-Friedrichs-Lewy (CFL) condition, defined in Eqn. (9). This criterion states that the non-dimensional Courant number must be less than unity, indicating that the time step and mesh size must be designed such that the amplitude of a wave traveling across the domain can be fully resolved within one computational cell [19]. Here, because the discretization method is implicit and thus inherently stable, the Courant number served as a preliminary measure of simulation accuracy. However, meeting the Courant criterion imposed severe computational overhead with full-scale simulations requiring upwards of 20 hours for 0.3 seconds of simulation time. Thus, to improve computational efficiency, the time step was increased such that the mean Courant number across the domain remained bounded and results agreed with tests in which Co remained below unity. This timing study will be discussed in more detail in the *Convergence Study* section.

$$C = \frac{u\Delta t}{\Delta x} \tag{9}$$

D. DEM Sub-Model

The particle model in this simulation uses a single input script to define the particle type, properties, computational domain parameters, and cohesion model. This simulation uses a granular atom style, which allows for the appropriate particle data to be associated (diameter, mass, and angular velocity), as well as thermal and cohesion properties which are associated with all atom styles [20]. Material properties (Young's Modulus, Poisson's Ratio, restitution coefficient, and friction coefficient) are all defined to correspond with the appropriate particles used during testing. The computational domain is defined using the external walls of the CFD mesh, with a sub-domain defined for the particle insertion sub-script, which inserts atoms into the main chamber according to a defined density function and allows them to settle into a loosely packed bed due to gravity.

The general granular interactions are modelled using Eqn. (10), which defines the forces between two neighboring particles [21]. These forces occurring when the distance between particle centers is less than their contact distance (ie. contact forces) and when the particle surfaces do not touch (ie. cohesion forces). The base model is characterized by a normal force consisting of contact ($k_n\delta n_{ij}$) and damping forces($\gamma_n v n_{ij}$) and a tangential force consisting of shear ($k_t\delta t_{ij}$) and damping forces ($\gamma_t v t_{ij}$) between particles. These are defined by elastic (k) and viscoelastic (γ) material constants to define the contact and damping forces. The cohesion effect is accounted for using a simplified Johnson-Kendall-Roberts model, which adds an additional term to the normal force interaction, Eqn. (11), to account for cohesion energy that tends to maintain atom contact, based on the particle contact area, A, and cohesion energy density, k [22].

$$F = (k_n\delta n_{ij} - \gamma_n v n_{ij}) + (k_t\delta t_{ij} - \gamma_t v t_{ij}) \tag{10}$$

$$F_n = k\,(2\pi\delta_n(2R)) \tag{11}$$

The DEM time step is defined by two time step criteria, which are derived from the particle collision event, and both of which are defined for the Hertzian contact model used here. The first is the Rayleigh time criterion, based on the time required for elastic wave propagation which occurs during particle collisions, seen in Eqn. (12) [23]. The second is the Hertz time criterion, which is defined by the theoretical duration of contact between two spherical particles predicted by the Hertz-Mindlin contact theory, seen in Eqn. (13) (this criteria is unnecessary in this simulation because the particle velocities are so low) [23]. To ensure stability of the DEM simulation, the particle time step was calculated to be 1e-3 seconds, $\sim$10% of the calculated Rayleigh time.

$$dt_r = \pi r \frac{\sqrt{\frac{\rho}{g}}}{0.1631\nu + 0.8766} \tag{12}$$

$$dt_h = 2.87\left(\frac{m_{eff}^2}{r_{eff}Y_{eff}^2 v_{max}}\right)^2 \tag{13}$$

E. CFD-DEM Coupling

As previously discussed, the coupling between DEM and CFD simulation occurs at set intervals. Here, to enforce a strong coupling between fluid and particle phases, the coupling interval is selected to be 10. This means that the two-way coupling between DEM and CFD solvers occurs every 10 DEM timesteps (1e-2 sec). During this phase, momentum transfer between fluid and particle phases occurs, and particle-fluid interactions forces are calculated. As seen in Eqn. (5) and Eqn. (6), the particle-fluid interactions forces, which are dominated by the drag, pressure gradient, and viscous forces, appear in both CFD and DEM momentum conservation equations. Further, the conservation equations for the fluid phase also take into account the particle void fraction and particle-velocity in each cell (if particles are present). In the CFD solver, an implicit momentum source term, K_{pf} is used to account for these factors, where F_{pf} is the sum of the particle-fluid interaction forces [20].

$$K_{pf} = \frac{\alpha_f \mid \sum_i \mathbf{F_{pf}} \mid}{V_{cell} \mid \mathbf{u_f} - \mathbf{u_p} \mid} \tag{14}$$

Since the system modelled here is approximated as a fluidized bed in the initial stages, the Koch-Hill drag force model was implemented in this simulation, Eqn. (15), with empirical correlations for F_0 and F_3 given in [24]. This model was developed using lattice-Boltzman simulations, and has been shown to well approximate drag force for spouting and fluidized beds [25].

$$\beta = \frac{18\mu_f \varepsilon_f^2 \varepsilon_p}{d_p^2} \left(F_0(\varepsilon_p) + 0.5F_3\varepsilon_p Re_p\right) \tag{15}$$

IV. Simulation Results

In this simulation testing, two different geometries were used. First, a reduced section of the geometry, as indicated in Fig. (1), was tested to verify the (1) base solver stability, (2) quantitative accuracy of the outlet fluid properties as compared with a separate compressible fanno flow analysis and commercial compressible flow CFD simulations (not described in this report), and (3) qualitative accuracy of the bulk particle movement as compared with experimental videos. Then, the full system geometry was simulated to verify (1) the quantitative accuracy of the particle velocity profile in the downstream tube section as compared to experimental data, and (2) downstream fluid velocity trends as compared to compressible fanno flow analysis and compressible flow simulations. A convergence study was also completed to analyze the mesh- and timestep-independence of the simulation, and to verify that larger CFD timesteps could be used to decrease computational time while still maintaining accuracy. Finally, a sensitivity analysis was completed, to analyze how the model outputs changed as a function of the particle coefficient of restitution, α_{COR}, which is not easily characterized.

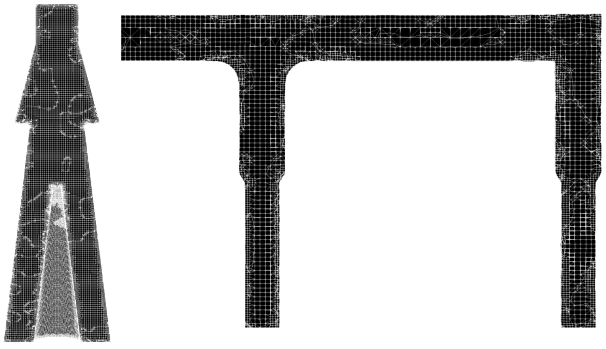

Fig. 3. Half-section of the hex-tet mesh generated for the reduced geometry system (L) and detailed downstream mesh for full system geometry, including outlet and secondary chamber (R)

To validate the incompressible simulation results, analytical calculations using compressible fanno flow analysis and a compressible flow simulation (using the commercial CFD solver, Ansys Fluids) were completed. The fanno flow analysis and compressible flow simulation were in good agreement, predicting that the outlet velocity past the annulus, would rapidly accelerate to reach approximately 60-70 m/s. The compressible flow simulation also showed that density across this reduced domain remains approximately constant, so the incompressible flow simulation described here should be valid.

A. Reduced Geometry

Using the simulation parameters described in the previous section, the reduced geometry simulation showed high stability and converged towards the expected velocity profile. Using the fluid density predicted from the compressible flow analyses, mean steady-state outlet velocity is approximately 60-70 m/s, which agrees with that predicted by the compressible flow analyses (55-65 $\frac{m}{s}$), validating the base CFD sub-model. (Both reduced and full system geometries are showed in Fig 4 for comparison).

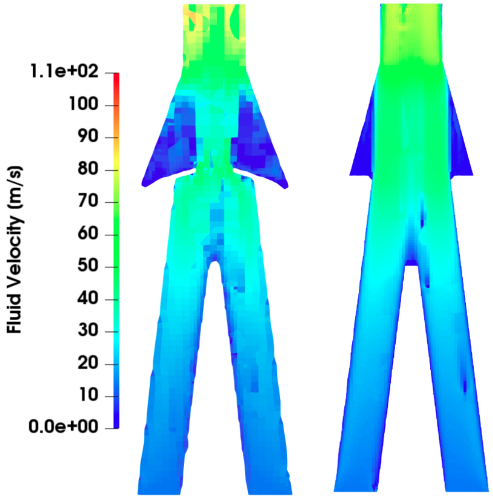

Fig. 4. Velocity profile in initial chamber at 0.125 seconds for reduced geometry (left) and full system (right)

The predicted bulk particle movement also closely matched the experimentally observed transport behavior. The bed immediately fluidizes and all of the particles are evacuated out of the annulus chamber, with some particles cohesively attaching to the outer walls of the chamber and the intermediary outlet ledge. Transient behavior can be seen in Fig. (5). (Data from experiments has not been cleared for release and so cannot be shown here for comparison).

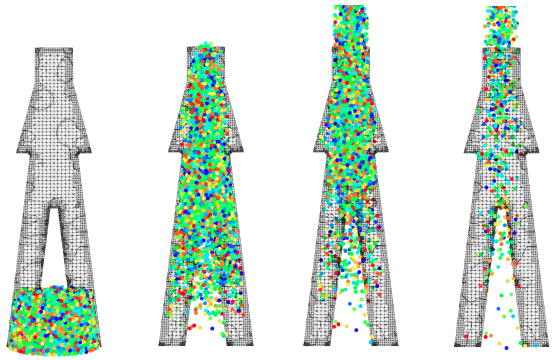

Fig. 5. Particle behavior in the reduced geometry simulation model at t = 0.001, 0.05, 0.08, 0.125 seconds

B. Full Geometry

Following the completion of the reduced geometry simulations, the full system geometry was simulated, comparing particle velocity profile in the downstream tube section as compared to experimental data, and downstream fluid velocity trends as compared to compressible flow analyses. Note that this simulation was completed using the same model parameters and pressure boundary conditions, since in incompressible flow simulations, the pressure is relative (ie. only the pressure gradient matters, not absolute pressure).

As seen in Fig. (6), axial particle velocity through the downstream tube reached 5-6 m/s, also matching with the experimental data velocity data (calculated using image processing of testing videos). The downstream fluid velocity trends also agreed with the compressible flow simulations, showing a sharp acceleration immediately past the branch in the tee (though exact numbers differed due to the incompressible flow assumption). Finally, the bulk particle movement agreed with the experimental data, with similar particle distributions in the two collection chambers.

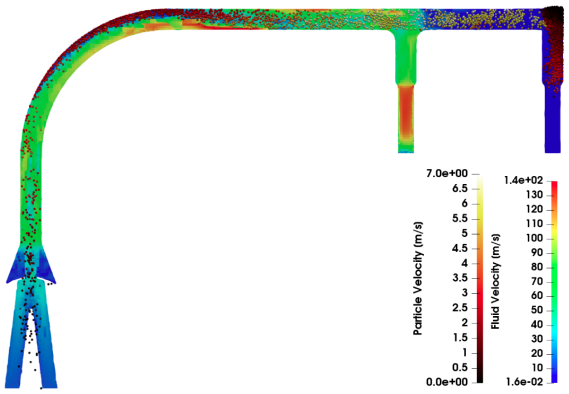

Fig. 6. Fluid and particle velocity profile, demonstrating downstream particle collection behavior, in the full system geometry simulation (t = 0.125 sec.)

C. Convergence Study

To verify that this model is mesh- and timestep- independent, a convergence study was completed to analyze the transient response of the fluid pressure gradient in the reduced geometry system.

To verify mesh-independence, "coarse" and "fine" CFD domains were generated by varying resolution of the base hex block domain. The coarse mesh used approximately 1e5 cells, while the fine mesh used around 5e5 cells. Both ran with the same timestep (2e-5 sec). This increased the CFD domain resolution greatly, while maintaining similar mesh quality as defined by average cell non-orthogonality and skewness.

The transient velocity profiles of both mesh types can be seen in Fig 8. Both simulations showed similar qualitative behavior, but the finer mesh exhibited a "delay", likely due to increased time required to fully capture fluid velocity in the particle-fluid momentum balance. Because the main model output of interest was particle behavior, this was deemed to be acceptable for this preliminary model.

In testing timestep-independence, the large and small timesteps were set to $dt = 1e-4$ and $dt = 1e-6$ seconds,

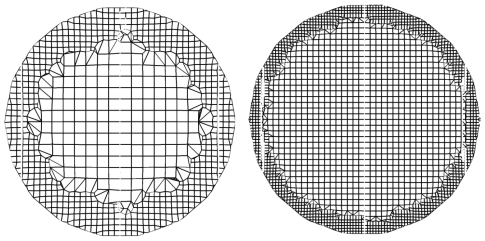

Fig. 7. Comparison of mesh resolution at the outlet: Coarse (L) and fine (R)

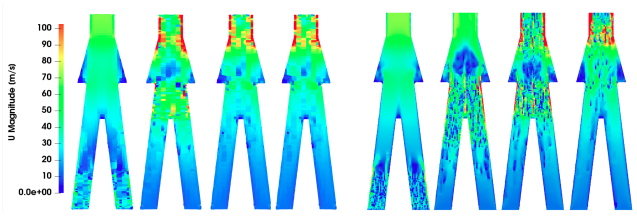

Fig. 8. Velocity profile [$\frac{m}{s}$] at t = 0.001, 0. 05, 0.08, 0.125 sec for coarse (L) and fine (R) mesh

respectively. In the small timestep case, the mean Courant number hovered around 0.18, while the mean Courant number for the large timestep remained stable around 0.96. The transient pressure gradient of both mesh types can be seen in Fig 9. Both models showed very similar transient results, with only minor variations (<5-10%) as the bulk particle mass moved out of the initial annulus, indicating that the model is relatively timestep-independent. Both convergence studies suggest that the fluid behavior can be adequately captured, even at Courant numbers that are higher than usual, given that the primary goal of this model is to characterize bulk particle movement.

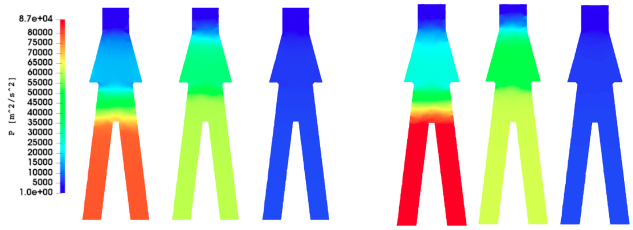

Fig. 9. Fluid pressure [$\frac{m^2}{s^2}$] at t=0.05, 0.08, 0.125 sec. for $dt = 1e-4$ (L) and $dt = 1e-6$ (R) sec.

D. Sensitivity Analysis

To test the model dependence on particle properties, the particle coefficient of restitution, α_{COR}, was varied between 0.1 and 0.5. This property varies based on material type, impact velocity, and impact history, so it is difficult to characterize. Steady-state particle distribution was analyzed for the full-system model (since that is the primary simulation output of interest in regards to particle data). Simulations showed extremely low deviation between the high and low α_{COR} values, with statistically negligible number of particles collected in the outlet chamber. This agreed well with experimental data. Representative steady-state particle distributions can be seen in Fig. (10).

Fig. 10. Particle distribution at $t = 0.125$ sec. for $\alpha_{COR} = 0.1$ (L) and 0.5 (R)

V. Conclusion

This paper has presented preliminary work completed on a coupled CFD-DEM model used to predict bulk particle movement in a hard vacuum environment, assuming cohesive, homogeneous particles and isentropic, incompressible, turbulent gas flow. This model was developed using open source modeling software (OpenFOAM, LIGGHTS, CFDEM-coupling), and detailed explanations have been provided for the base governing equations and model parameters, including fluid particle properties and coupling behavior. Preliminary results indicate that this low-fidelity model successfully validates hardware testing, providing a numerical tool which can be used to significantly accelerate the pneumatic system design workflow by reducing the physical testing required to iterate on designs, and provide a baseline comparison for future pneumatic conveying frameworks.

However, much work remains to be completed. Experimental data indicates that downstream of the initial annulus and chamber, closer to the outlet, the fluid density changes significantly and the fluid must be modeled as compressible. This agrees with general intuition, given that the gas is expanding into vacuum at the outlet. Thus, the incompressible CFD sub-model, while useful to visualize general fluid behavior, should be converted into a compressible flow model to more accurately capture the true system physics. In addition, the particle-fluid drag model used here (the Koch-Hill model) has primarily been validated for spouting and fluidized beds, with high solid void fraction. To better capture downstream particle-fluid interaction forces, the drag model should be dependent on the computational domain in which the particle resides - as the particle moves into the downstream pipe system, the drag model should shift into one more appropriate for pneumatic conveying systems. Finally, a higher-fidelity particle cohesion model can be implemented to more accurately capture particle-particle interactions. While the Johnson-Kendall-Roberts sub-model is while widely used in fluidization simulations, the sub-model parameters have not been finely tuned for this specific material, and particle aggregation, a behavior which can greatly affect the downstream particle interactions and bulk movement, is not considered.

References

[1] H. Norouzi, *Coupled CFD-DEM Modeling Formulation, Implementation and Application to Multiphase Flows*. John Wiley 'I&' Sons, Ltd., 2016.

[2] G. E. Klinzing, F. Rizk, R. Marcus, and L. Leung, *Pneumatic conveying of solids: a theoretical and practical approach*. Springer Science & Business Media, 2011.

[3] H. Enwald, E. Peirano, and A.-E. Almstedt, "Eulerian two-phase flow theory applied to fluidization," *International Journal of Multiphase Flow*, 1996.

[4] C. Moliner, F. Marchelli, N. Spanachi, A. Martinez-Felipe, B. Bosio, and E. Arato, "Cfd simulation of a spouted bed: Comparison between the discrete element method (dem) and the two fluid model (tfm)," *Chemical Engineering Journal*, 2019.

[5] L. Lu, X. Liu, T. Li, L. Wang, W. Ge, and S. Benyahia, "Assessing the capability of continuum and discrete particle methods to simulate gas-solids flow using dns predictions as a benchmark," *Powder Technology*, 2017.

[6] K. Hettiaratchi, S. Woodhead, and A. Reed, "Comparison between pressure drop in horizontal and vertical pneumatic conveying pipelines," *Powder technology*, 1998.

[7] I. V. Gould *et al.*, "Vacuum-pneumatic conveying of raw wool," in *Agricultural Engineering Conference 1982: Resources, Efficient Use and Conservation; Preprints of Papers*. Institution of Engineers, Australia, 1982.

[8] C.-Y. Wu and Y. Guo, "Numerical modelling of suction filling using dem/cfd," *Chemical engineering science*, 2012.

[9] Y. Guo, K. Kafui, C.-Y. Wu, C. Thornton, and J. Seville, "A coupled dem/cfd analysis of the effect of air on powder flow during die filling," *AIChE journal*, 2009.

[10] S. Jackson, I. Sinka, and A. Cocks, "The effect of suction during die fill on a rotary tablet press," *European journal of pharmaceutics and biopharmaceutics*, 2007.

[11] P. Reiss, P. Hager, A. Hoehn, M. Rott, and U. Walter, "Flowability of lunar regolith simulants under reduced gravity and vacuum in hopper-based conveying devices," *Journal of Terramechanics*, 2014.

[12] P. Breuninger, D. Weis, I. Behrendt, P. Grohn, F. Krull, and S. Antonyuk, "Cfd–dem simulation of fine particles in a spouted bed apparatus with a wurster tube," *Particuology*, 2019.

[13] Z. Zhou, S. Kuang, K. Chu, and A. Yu, "Discrete particle simulation of particle–fluid flow: model formulations and their applicability," *Journal of Fluid Mechanics*, 2010.

[14] C. Greenshields, "Openfoam v6 user guide: 4.1 openfoam case directory," Jul 2018.

[15] C. Goniva, C. Kloss, N. G. Deen, J. A. Kuipers, and S. Pirker, "Influence of rolling friction on single spout fluidized bed simulation," *Particuology*, 2012.

[16] R. I. Issa, "Solution of the implicitly discretised fluid flow equations by operator-splitting," *Journal of computational physics*, 1986.

[17] H. Versteeg and W. Malalasekera, "An introduction to cfd. the finite volume method," 2007.

[18] M. R. Hestenes, E. Stiefel *et al.*, "Methods of conjugate gradients for solving linear systems," *Journal of research of the National Bureau of Standards*, 1952.

[19] R. Courant, K. Friedrichs, and H. Lewy, "Über die partiellen differenzengleichungen der mathematischen physik," *Mathematische annalen*, 1928.

[20] K. Kloss, "Models, algorithms and validation for opensource dem and cfd-dem," *Progress in Computational Fluid Dynamics*, 2012.

[21] "pair_style gran command."

[22] "gran cohesion sjkr2 model."

[23] S. J. Burns, P. T. Piiroinen, and K. J. Hanley, "Critical time step for dem simulations of dynamic systems using a hertzian contact model," *International Journal for Numerical Methods in Engineering*, 2019.

[24] M. S. Van Buijtenen, W.-J. Van Dijk, N. G. Deen, J. Kuipers, T. Leadbeater, and D. Parker, "Numerical and experimental study on multiple-spout fluidized beds," *Chemical engineering science*, 2011.

[25] F. Marchelli, Q. Hou, B. Bosio, E. Arato, and A. Yu, "Comparison of different drag models in cfd-dem simulations of spouted beds," *Powder Technology*, 2020.